Swarm-mediated phage transport disrupts a biofilm inherently protected from phage penetration

Authors. Nichith K. Ratheesh, Cole A. Calderon, Amanda M. Zdimal and Abhishek Shrivastava

Affiliations. Biodesign Center for Fundamental and Applied Microbiomics, School of Life Sciences, Center for Biological Physics, Arizona State University, Tempe, 85281

Corresponding author. Abhishek Shrivastava

Email. ashrivastava@asu.edu

Keywords. Biofilm, phage therapy, active transport, swarming, bacterial motility, collective motion, microbiota

Abstract. Phage therapy, i.e., the treatment of chronic bacterial infections by virus that kill bacteria has shown promise in combating antimicrobial resistance (AMR). A typical phage particle is around 100 times bigger than a typical antibiotic molecule. Due to larger size, a phage particle diffuses slower than an antibiotic molecule, and can get trapped in the polymeric mesh of biofilm matrix. We report that a swarm of *Capnocytophaga gingivalis*, a bacterium abundant in the human oral microbiota, can actively transport phages over long distances. By tracking fluorescently labeled lambda phages that do not infect *C. gingivalis*, we demonstrate active predator transport by a *C. gingivalis* swarm. As a result, the rate of disruption of the prey, i.e., an *Escherichia coli* colony increases 10 times. Production of curli fiber by a mature *E. coli* biofilm blocks the intercellular space and is known to inhibit the diffusion of phages within a biofilm. We find that *C. gingivalis* forms tunnels within the prey biofilm. When phages are actively delivered, curli fiber containing *E. coli* biofilms are no longer protected against phage infection. Our results demonstrate that active delivery of the predator by a self-propelled swarm might improve the pharmacokinetics of phage therapy. This can lead to the development of a tool to combat chronic AMR biofilms.

Introduction

Antimicrobial resistance (AMR) is a global public health threat. In the United States alone, AMR results in over 35,000 deaths and 2.8 million cases every year[1]. The development of new antibiotics is a glacially slow process, and there is an urgent need to find alternative treatments for chronic bacterial infections. Biofilms are the culprits behind chronic burn wound infection, urinary tract infection, otitis media, and cystic fibrosis. Formation of biofilm by bacterial cells results in 10-1000 fold increase in antibiotic resistance[2]. Phage i.e., virus that kill bacteria are promising alternatives for antibiotic treatment during chronic AMR infections[3–6]. Multiple clinical trials to study

the application of phage therapy for infectious diseases are currently ongoing. A recent clinical trial reported that phage therapy resulted in the treatment of drug-resistant disseminated *Mycobacterium abscessus* infection in a patient with cystic fibrosis[7]. Similarly, phage therapy has successfully treated patients with chronic ear infection (otitis media) caused by antibiotic-resistant *Pseudomonas aeruginosa*[8] and infection of the urinary tract by *E. coli*, *P. aeruginosa*, *Streptococcus* spp., and *Enterococcus* spp[9]. Phage therapy has also been successful in treating *P. aeruginosa* infections in mouse burn wound models[10,11]. One limitation of phage therapy is that phage particles can get trapped in the matrix of infectious biofilms and their frequency of an encounter with a bacterial cell diminishes. This dilutes the effective concentration of the phage cocktail used for therapy. Topical application of phages was the delivery route used by a recent clinical trial for treating burn wound infections. This clinical trial was limited by low concentration of phages, and no improvement in infection after phage therapy was observed. In this trial, lower concentration was attributed to storage instability of phages[12]. It appears intuitive that in future, an additional clinical trial with higher phage concentration is needed for potential treatment of burn wound infections. Additionally, an improvement in the pharmacokinetics of phage therapy can help mitigate the barriers that arise due to lower phage concentration. In this article, we describe a novel approach to improve the efficiency of phage delivery within a biofilm

The larger size of phages as compared with antibiotic molecules results in a slower diffusion rate[13]. According to the Stokes-Einstein equation, the translation diffusion coefficient (D) of sphere of radius r in a medium of viscosity η is ${K_B T}/{6\pi\eta r}$ where K_B is the Boltzmann's constant and T is the absolute temperature. Higher D results in diffusion with a faster speed. The inverse relationship between D and r

implies that small molecules diffuse faster. One of the largest known antibiotic vancomycin (~1 nm radius) has 66 C atoms[14]. The Carbon chain length of most commonly used medicinal antibiotics are about a quarter to half of vancomycin. For eg., amoxicillin and cefalexin have 16 C atoms, ciprofloxacin and methicillin have 17 C atoms, and azithromycin has 38 C atoms[15–18]. The capsid of lambda phage used in our study has a radius of about 30 nm[19] while *Cystovirus* that infect *Pseudomonas* sp. have a radius of about 40 nm[20]. This suggest that *Cystovirus* will diffuse 40 times slower than vancomycin. Based on the Carbon chain length, if one estimates cefalexin it to be a quarter of the size of vancomycin, *Cystovirus* will diffuse 160 times slower than cefalexin. Similarly, lambda phage will diffuse 100 times slower than cefalexin and 30 times slower than vancomycin. In order to establish phage therapy as a widely-used efficient alternative to antibiotic treatment, one needs to overcome its diffusion-based limitation.

The data presented in this article suggests that active transportation of phages by a swarm of motile bacteria can help overcome the physical constraints and diffusion based limitations of phage infection. Our approach increases close encounters between phages and infectious bacterial cells. The bacteria used as 'transporters' in our study belong to the genus *Capnocytophaga* and are found in abundance in the oral microbiota of healthy humans, suggesting that they may show promise as probiotics.

Non-motile bacterial species are known to hitch a ride on motile bacterial species. Swarms of *Paenibacillus vortex* transport non-motile bacteria to navigate through toxic environment, where *P. vortex* acts as a means of transport and the other species degrade the toxic products present in the environment[21]. This is a classic example of

protocooperation among bacterial species. However, sometimes commensalism, where only one interacting species reap benefits from the interaction is also observed. Examples include the transport of nonmotile bacteria[22] and spores[23] by swimming bacteria, gliding bacteria[24], and zooplankton[25]. Electron microscopy images have shown that phage particles bind to bacterial flagella[26] and imaging of colonies infected by the phage suggests hitchhiking[26,27]. Do non-flagellated but motile bacteria transport phage particles and can one directly visualize phage transportation? We sought to answer this question with the help of *Capnocytophaga gingivalis*, which is a member of the bacterial phylum Bacteroidetes. *C. gingivalis* exhibits gliding motility and transports non-motile bacterial species of the human oral microbiota. Cargo transportation by *C. gingivalis* shapes the spatial organization of a microbial community[24].

Swimming, twitching and gliding are the three major modes of motility exhibited by bacteria[28,29]. Bacterial gliding is an active process and individual rod-shaped gliding bacteria move in a screw-like fashion[30,31]. Bacteria of the phylum Bacteroidetes are among the abundant members of the healthy human microbiome. Motile members of the phylum Bacteroidetes exhibit gliding motility with the help of the Type 9 Secretion System[32,33]. Bacteroidetes gliding motility is driven by a rotary motor[34] that couples with a cell-surface track[35]. *C. gingivalis* moves over an external surface with the help of a cell surface adhesin SprB[35]. On an agar surface, cells of *C. gingivalis* and related gliding bacteria swarm in a vortex-like fashion[24,36]. In the fluid layer that surrounds the swarm, buoyant particles such as gas bubbles can be transported over long distances[24].

Our results show that fluorescently labeled lambda phage particles are transported by a swarm of *C. gingivalis.* Lambda phage is a predator of *E. coli* and it does not infect *C. gingivalis*. We find that due to phage transport, the rate of disruption of an *E. coli* colony increases 10 times as compared with a control where phages were simply diffusing. Recently, it was shown that the presence of curli fiber obstructs the diffusion of phages within an *E. coli* biofilm[37]. Curli fiber is an amyloid protein produced and excreted by biofilm forming cells and it increase cellular aggregation[38]. Curli fiber wraps around individual cells and it occupies intercellular space within a biofilm. As a result, curli fiber protects cells within a biofilm from phage infection[37]. When phages are actively delivered, curli fiber containing *E. coli* biofilms are no longer protected against phage infection. In a typical habitat, virus are 10 times more abundant than microbes[39]. Our results point towards a novel mode of cooperation between microbes and the viruses that share a habitat. In future, this interaction can be harnessed to improve the pharmacokinetics of phage therapy.

Results.

Our data show that a swarm of *C. gingivalis*, a bacterium that is abundant in the oral microbiota of healthy humans[40], can actively transport lambda phage particles over long distance (**Movie S1 and Fig. 1a, b**). The experiments were performed using lambda phage particles that have Yellow Fluorescent protein (YFP) attached to their coat protein gpD[41]. Lambda phage infects *E. coli* but it does not have the ability to infect *C. gingivalis* (**Fig. S2**). We found that a swarm of *C. gingivalis* provides an efficient tool for phage delivery.

Motility of the gliding bacterium *C. gingivalis* is driven by the rotary Type 9 secretion system (T9SS) and is fueled by a proton motive force[35,42]. T9SS containing bacteria

belong to the Gram negative Fibrobacteris-Chlorobi-Bacteroidetes superphylum. The outer membrane pore of T9SS is formed by the largest beta-barrel known in biology[43]. T9SS containing Bacteroidetes are abundant in the human oral and gut microbiota. A large cell-surface protein SprB acts as a focal adhesin and it facilitates T9SS driven bacterial gliding motility[35]. Besides aiding in motility, SprB also binds to non-motile bacterial species. Cargo transportation by *C. gingivalis* shapes the spatial organization of a polymicrobial community[24]. We found that phages were transported due to hydrodynamic swarm fluid flows generated by *C. gingivalis* (**Movie 1**). In most cases, a phage particle did not bind to a *C. gingivalis* cell (**Movie 2**). In very rare cases, we observe transient attachment of a phage to a *C. gingivalis* cell (**Movie 3 and Fig. S2**).

A bacterial swarm generates a thin layer of liquid called as the swarm fluid[44]. It is rich in osmotic agents and surfactants. Secretion of osmotic agents by swarming bacteria results in a gradient along which water moves out from the agar. Mixing of water with the osmotic agents and surfactants results in the swarm fluid. Surfactants secreted into the swarm fluid keep the swarming cells wet and help in reduction of water loss from the substratum[45]. By using microbubbles as tracers, it was shown that the fluid of an *E. coli* swarm moves orthogonal to direction of motion of the swarm front [44]. This was attributed to the fact that the direction of rotation of the *E. coli* flagella bundle is orthogonal to the long axis of the cell. In the case of gliding bacterium, the mobile adhesin SprB moves along the long axis of the cell. Hence, microbubbles move along the direction of motion of a *C. gingivalis* swarm. Tracking of phage particles showed that phages were transported by *C. gingivalis* in the direction of propagation of the swarm (**Fig. 1a, S1**). Phage particles were transported with a mean speed of 20 μm/minute (**Fig 1c, S1**), which is also the speed of motion of individual cells in a swarm[24]. Changes in Mean Square Displacement (MSD) as a function of time

provided a powerlaw slope of 1.22. Hence, the transport of phages by a *C. gingivalis* swarm is an active super-diffusive process **(Fig 1c)**.

It is predicted that around 10^{12} phages reside in the human gut[46]. Phages are abundant in the human oral microbiota and a 1 μL volume of saliva contains 100,000 virus-like particles[47]. *Capnocytophaga* isolates from the human oral cavity are robustly motile[48] and as we now know, they transport phages (**Fig. 1**). Viewing the abundance of phages in the light of our results suggest that swarm-mediated transport of predators can help shape the architecture of a microbial community. The human oral microbiota has a well-defined spatial structure[40]. It is possible that active phage transport might play a currently unexplored role in molding the architecture of the human oral microbiota.

Active phage transport can help improve the pharmacokinetics of phage therapy. To test if swarm-mediated phage transport provides an advantage over phage transport by diffusion, we performed stochastic simulations that are based on Fick's laws of diffusion. The predictions of our simulations were tested by experiments. In order to design a control for our experiment, it was necessary to find the diffusion constant of phages in a thin liquid surface layer of wet agar. We inoculated 2 μL of 10^8 CFU/mL fluorescent lambda phages over an agar surface and it was incubated in a 100% relative humidity chamber. Diffusing fluorescent phages in a thin liquid on the agar surface were imaged (**Movie S4**) and their MSD powerlaw slope was 0.68 (**Fig. 2a**), which suggests that the phages were sub-diffusive. The sub-diffusivity can be attributed to the viscosity of the thin liquid surface layer of the wet agar hydrogel and the adhesion of phages to agar. Using the Einstein relation[49] $D = {<\Delta r^2>}/{n\Delta t}$ we calculated the diffusion coefficient (D) of phages to be 0.041 $\mu^2 s^{-1}$. Here, Δr^2 is the

change in squared displacement, n is the dimensionality of the diffusion, and Δt is the change in time[49]. Using the Stokes-Einstein equation described in the introduction section of this article, we found that the viscosity (η) of a thin liquid layer on the wet agar hydrogel surface is 218 cP. Lambda phages have a radius of about 30 nm[19] and we performed a simulation to calculate the distance that a phage particle can diffuse in 30 hours. For this purpose, we used the Fick's second law of diffusion[49] ${\Delta C}/{\Delta t} = {D\Delta^2 C}/{\Delta x^2}$ where ΔC is the change in concentration, Δt is the change in time, D is the diffusion coefficient and Δx is the change in distance. Our simulations predict that at 33°C, phage particles will only diffuse a distance of 400 µm in 30 hours (**Fig. 2b**), and this in-silico result guided the design of the wet-lab experiment shown in Fig. 2d and described later in this text. For comparisons of the in-silico result, we simulated the diffusion of lambda phage particles in lesquerella oil that has a reported viscosity (275 cP at 23.9°C)[50] that is similar to our control. To find the viscosity of the swarm fluid of *C. gingivalis*, 2 µL of 10^8 CFU/mL fluorescent phages were spotted on top a 72 hour old post-swarm *C. gingivalis* colony. Around 72 hours, *C. gingivalis* stops swarming and the diffusion of fluorescent phages on a post-swarm colony was captured via confocal microscopy. The MSD powerlaw slope was 0.405 (**Fig. 2A**). As described above, the viscosity of fluid on the surface of a post-swarm colony was calculated to be 994 cP at 33°C. For further comparison, we simulated the diffusion of lambda phage particles in canola oil that has a reported viscosity (61 cP at 40°C)[51] that is much lower than our control. As shown by our simulations, phages will diffuse faster in liquids of lower viscosity and vice-versa. It appears that the thin liquid layer on the surface of a wet and saturated agar hydrogel has viscosity slightly higher than lesquerella oil but lower than canola oil (**Fig. 2b**).

C. gingivalis swarm in a circular fashion wherein new circles propagate from the edge of an initial circular swarm[24]. The total distance that a bacterium moves within a circular swarm can be calculated by measuring its circumference $(2\pi r)$. The one dimensional distance traveled by the bacterium during one full circular vortex of the swarm is equal to the diameter of the circle. The known speed of a swarm that moves in a circular pattern (20 μm/min)[24] can be converted to a 1-dimensional rate of motion by dividing the circular speed by π i.e., the ratio between circumference and diameter. This results in an effective 1 dimensional speed of 6.36 μm/min. This 1 dimensional speed is the effective advective velocity v_d of the swarm.

Using the advection-diffusion equation[49] $\partial C/\partial t = D\,\partial^2 C/\partial x^2 - v_d\,\partial C/\partial x$ we found that *C. gingivalis* can transport phage particles to a distance of ~1500 μm in 3.3 hours (**Fig. 2c**). Here, C is the concentration of phages, t is time, x is distance, D is the diffusion coefficient, and v_d is advective velocity. *C. gingivalis* starts swarming about 7 hours after initial inoculation on an agar surface. Due to the output of our simulation (**Fig. 2C**), during the wet-lab experiment, we provided the swarm 3 hours for phage delivery. We started capturing images 10 hours after the initial inoculation. This provided 7 hours for swarm initiation and 3 hours for phage delivery. To capture the death of *E. coli* after interaction with the delivered phages, we kept imaging for an additional 21 hours (**Fig. S3, 4, 5**).

We inoculated phage-CG mix (10 μl of fluorescent phage lysate added to 20 μL of C. *gingivalis* suspension, see methods) and *E. coli* MG1655 with pBT1 mcherry on a wet agar surface at a distance of 1000 μm. The samples were incubated in the presence of 100% relative humidity. Via confocal microscopy, changes in *E. coli* biomass were measured over a period of 30 hours. As controls, similar volumes of either 10^8 CFU/mL of lambda phage or *C. gingivalis* suspension were separately

spotted at a distance of 1000 μm from a fluorescent *E. coli* colony. We found that in the control, some phages diffuse to the edge of the *E. coli* colony. This can be attributed to fluid flows created by the addition of cover glass. Samples were imaged 500 μm inwards from the edge of the *E. coli* colony. In this region, minimal reduction in *E. coli* biomass was observed in the control (**Fig. 2c, e**). This implies that artificial fluid flows that might get created during sample preparation can't deliver phages to this region. The effective distance at which we were imaging the colony was 1500 μm (1000 μm distance between the spots + 500 μm inwards from the edge of the *E. coli* colony) from the source of phage and/or *C. gingivalis*. Our simulation for advective diffusion shows that *C. gingivalis* can transport phages to a distance of 1500 μm in 3.3 hours (**Fig 2c**). Our simulation also shows that phages can only diffuse a distance of 400 μm in 30 hours (**Fig 2b**). This in-silico outcome was captured in our experiment where we found that the biomass of *E. coli* does not change in our control (**Fig. 2d, e and Movie 6**). In contrast, when phages were actively transported by *C. gingivalis*, the *E. coli* biomass reduction occurs 10 times faster (**Fig. 2d, e and Movie 7**). No change in *E. coli* biomass was observed when *C. gingivalis* alone was spotted at a distance of 1000 μm from the *E. coli* colony (**Fig. S5 and Movie 8**). This shows that inter-bacterial competition due to metabolites or physical forces do not play a role in the reduction of biomass of *E. coli*. The phenotype that we report serves as a novel example of predator-prey relationship in the microbial world.

Recently, Vidakovic and co-workers demonstrated that a polymeric mesh generated by curli fiber creates a physical barrier that protects a biofilm from phage infection[37]. In order to test if active phage transportation can bypass the physical barrier created by curli fiber, we introduced *C. gingivalis* near the circumference of a curli fiber-producing mature *E. coli* biofilm. We found that in the presence of active

transportation, phages were able to penetrate through the biofilm. Strikingly, some phages even reached the bottom of the biofilm (**Fig 3d-f**). In the absence of *C. gingivalis,* most phages were concentrated at the top layer of the biofilm (**Fig 3a-c**). In our experiment, we found that the greatest number (5.1 X 10^4 phage particles, by calculating the phage area in each 2d image of the z-stack and dividing it by the area of a single phage particle) of phages were found at a depth of about 60 μm of a biofilm that has a total height of 105 μm (**Fig 3i**).

As shown in fig. 4, we find that *C. gingivalis* forms tunnel-like structures within an *E. coli* biofilm. Single cells of *C. gingivalis* and other closely related bacteria move in a screw-like fashion[24,30]. It is possible that this self-propelled screw enables phage invasion by drilling tunnels into a biofilm with curli fiber. In a swarm, multiple self-propelled screws might work towards drilling a common tunnel. In order to test if *C. gingivalis* can form tunnel-like structures, we introduced *C. gingivalis* near the circumference of the curli fiber-producing mature *E. coli* biofilm. The samples were incubated for sufficient time that allows *C. gingivalis* to swarm over an *E. coli* biofilm. *C. gingivalis* cells were stained by Fluorescence *in situ* hybridization (FISH) and *E.coli* had cytoplasmic mcherry. The total height of the *E. coli* biofilm was 105 μm but *C. gingivalis* only formed tunnels within a 50 μm thick zone (**Fig 4c**). The zone preferred by *C. gingivalis* spans from 20 μm depth to 70 μm depth from the top of the *E. coli* biofilm. It must be noted that the maximum phage penetration after active transportation was observed at a depth of around 75 μm (**Fig 4a, b**). Our results point towards a novel mechanism for phage delivery where a self-propelled screw drills holes in a biofilm and drives a thin layer of fluid that carries phages to their targets.

Discussion.

As demonstrated by our results, active transportation increases the frequency of interaction between the predator and the prey. While our work improves the fundamental understanding of microbial ecology, it can also be applied to improve the pharmacokinetics of phage therapy. Additionally, this newly discovered mode of phage delivery can be further optimized by the fine tuning of chemotaxis. *C. gingivalis* is an understudied bacterium and very little is known about its chemotaxis pathway. The genome of *C. gingivalis* encodes a homolog of the chemoreceptor Aer[52] and *C. gingivalis* swarms best in CO_2 rich microaerophilic conditions. It might be possible that via Aer, *C. gingivalis* senses intracellular energy levels and is guided towards a location that allows for a preferred redox environment. Chemotaxis of flagellated bacteria is well-studied and is known to impact autoaggregation[53,54], symmetrical pattern formation and traveling wave formation[55–57]. Increased physical interactions between cells in a swarm reduces the ability for tracking of chemotactic gradients[58] but the chemotaxis pathway can also be remodeled for swarming[59]. In fig. 4a, we find that most of the *C. gingivalis* is found between the depth of 20 to 70 μm of the *E. coli* biofilm. It might be possible that chemotaxis of the transporter drives preferential localization of the predator within a biofilm of prey. Topical application of phage is the preferred method for treating burn wound infection, and our results (**Fig. 3 and 4**) demonstrate improved delivery of topically applied phages within an in-vitro *E. coli* biofilm. Topical application of phages has shown success in treating patients with antibiotic-resistant *Pseudomonas aeruginosa* in chronic ear infection (otitis media)[8]. The preferred mode of phage delivery varies according to the site of infection. Phages have been delivered via intravenous injection to treat a 15-year-old cystic fibrosis patient with a disseminated *Mycobacterium abscessus* infection[7]. Via a suprapubic catheter, phages were delivered to treat patients with urinary tract infection[9].

Additionally, efforts are being made to deliver phages to pulmonary infections via a nasal spray[60]. The potency of all current methods of phage delivery can be improved by the formation of tunnels within infectious biofilms. As shown by our results, tunneling via a swarm can deliver phages to previously inaccessible regions within a biofilm. Furthermore, active transportation of phages via a bacterial swarm might speed up the recovery of a patient. In future, chemotactic control of the directionality of a swarm can help expand active phage delivery to chronic biofilms that grow in relatively inaccessible locations within the human body.

We find that most phages are transported by the swarm fluid and there is very little interaction between individual transporter cells and phages. In future, *C. gingivalis* might be genetically manipulated to bind to specific phage proteins. While this approach will improve the binding, the overall efficiency of transport might not improve. It is possible that steric hindrances due to the binding to phage particle might impede screw-like motility of the transporter cell. Most clinical trials use a cocktail of phages for therapy. A universal phage transporter where phages do not impede motility is the best approach for the delivery of all phages in the cocktail. The natural habitat of *C. gingivalis* is the human oral microbiota. It does not escape our attention that bacterial swarms on gut and oral mucosal surfaces within the human body might be transporting virus particles that impact human health.

Methods.

Strains and Media. *Escherichia coli* MG1655 was grown on Luria-Bertani (LB) agar. The plasmid pBT1 mCherry (a gift from Michael Lynch, Addgene plasmid # 65823) was inserted via electroporation into *E. coli* MG1655. Cells were cultured on LB agar with 100 µg/mL ampicillin at 37°C. A single colony was inoculated in 3 mL LB broth

with ampicillin at 37°C and was grown overnight with shaking. Subsequently, a day culture was prepared by adding 300 µL of the overnight culture to 30 mL of LB broth with ampicillin. For a day culture, cells were grown to mid-log phase at 37°C shaking. *E. coli* WR3110 (gift from Knut Drescher, University of Basel) was grown on LB agar at 37°C. The plasmid pBT1 mCherry was inserted via electroporation into *E. coli* WR3110. To grow curli producing biofilms, *E. coli* WR3110 was spotted on trypticase soy broth (TSB) at 28°C for 48h.

Motile *Capnocytophaga gingivalis* ATCC 33624 were grown on TSB 30 g/L, yeast extract 3 g/L, and 1.5% Bacto Agar (Difco) as described previously[24]. Growth was carried out in a CO_2 rich anaerobic environment with 100% relative humidity. Briefly, inoculated agar plates were placed in an AnaeroPack System jar (Mitsubishi Gas Chemical) with an ignited sheet of Kimtech paper and a beaker full of water. The box was sealed and incubated at 37°C for 48 h. *C. gingivalis* suspension was prepared from 27µg of *C. gingivalis* culture scrapped off a 24h plate and adding 50µL of sterile water.

Preparation of phage lysate. The fluorescent phage λ_{LZ641} (gift from Lanying Zeng, Texas A&M University) used in this study contains a mixture of wild-type head stabilization protein gpD and a fusion of gpD with yellow fluorescent protein (eYFP)[61]. *E. coli* strain MG1655 was grown in LB broth with overnight shaking at 37 °C. 100 µL of the *E. coli* culture was mixed with 100 µL of either 10^{-6} or 10^{-7} dilution of a 10^{8} PFU/mL lysate stock of λ_{LZ641}. After incubation at room temperature for 15 minutes, the mixture was added to 4 mL top Agar (LB with 0.7% agar) (50°C), gently mixed and spread on a fresh LB agar plates. Plates were then incubated overnight at 37°C. Top agar was scraped off from plates with plaques, transferred into a microcentrifuge tube

with 1.2 mL of sterile water. The tubes were incubated for 4 hours at room temperature and centrifuged at 1900 rcf for 5 minutes. The supernatant containing phage particles was transferred into a fresh sterile microcentrifuge tube and kept at 4°C for immediate use and -20°C for long-term storage. For a plaque assay, similar method as above was performed with either an *E. coli* culture or a *C. gingivalis* suspension. Top agar plates were incubated at 37°C in presence of the above described growth condition for the host bacterium.

Data and Image Analysis. All custom data and image analysis scripts are freely available at https://github.com/krNichith/Phage-delivery

Analysis of phage transportation. 10 µl of fluorescent λ_{LZ641} phage lysate was added to 20 µL of C. *gingivalis* suspension. During the rest of our text, we will refer to it as the phage-CG mix. 2 µL of the phage-CG mix was spotted on a TSY agar pad and incubated for 5 minutes at room temperature. Subsequently, a coverslip was placed, and the edges are sealed using beeswax (Aqua Solutions, Inc. Lot#: 730701). The slides were incubated in a humid AnaeroPack System box described above. The box was sealed and incubated at 37°C for 3 hours.

Images were captured with the Zeiss LSM880 confocal microscope (Oberkochen, Germany) and phages were tracked using an ImageJ plugin TrackMate. The 2-dimensional position coordinates of each phage particle were exported from ImageJ in a .xml format. The .xml files were imported using MATLAB and converted to a .csv file. The .csv file was imported using Python and converted to a DataFrame. Mean speed and mean square displacement (MSD) of each phage particle were calculated using custom Python scripts.

To test if phages attach to individual *C. gingivalis* cells, 50 µL of a 1:1 mixture of *C. gingivalis* and λ_{LZ641} was injected into a tunnel slide. The tunnel slide was inverted and

incubated at room temperature for 5 minutes. This was followed by adding 50 μL of 10% methyl cellulose. After an additional 5 minutes of incubation, single *C. gingivalis* cells and fluorescent phages were imaged near the cover glass by a Zeiss LSM880 confocal microscope . Images were analyzed using ImageJ.

Change in biomass of *E. coli* colony after phage delivery. *E. coli* MG1655 containing plasmid pBT1 mCherry was grown overnight shaking at 37° C. 1 mL of the culture was pelleted and resuspended in 250 μL of sterile water. 2 μL of this suspension was spotted on a fresh TSY agar plate. 2 μL of phage-CG mix was spotted at a distance of 1 mm from the *E. coli* spot. The plate was incubated in a humid AnaeroPack System box described above. The box was sealed and incubated at 37°C for 10 hours. After incubation, a circular slab of agar surrounding the colony was cut with a scalpel and transferred on to a smaller petri plate (35 X 10 mm). A coverslip was placed and the edges were sealed using beeswax. Using a Zeiss LSM880 confocal microscope, time-lapse images were obtained for the next 21 hours. The interval between each image was 1 hour and the area of *E. coli* colony was calculated using the Python library Scikit-image. Change in biomass of the *E. coli* after phage delivery was determined via a custom Python script.

Assay of phage delivery within a mature *E. coli* biofilm. A curli-fiber producing *E. coli* strain WR3110 with plasmid pBT1 mCherry was grown on TSY agar pad for 48 hours at 28 ^{o} C. The lower temperature maximizes curli-fiber production and biofilm formation. A 50 μL *C. gingivalis* suspension was pipetted around the circumference of the mature *E. coli* biofilm and the plate was incubated in a humid AnaeroPack System box describe above for 14 hours at 37° C. Subsequently, 20 μL of 10^5 PFU/mL λ_{LZ641} was spotted on the biofilm and the plate was incubated for another 10 hours at 37° C in a humid AnaeroPack System box described above. After incubation, z-stack images

(3 μm slices) of the *E. coli* biofilm were obtained using a Zeiss LSM 880 confocal microscope. Z-stack images were analyzed via custom Python scripts that use Scikit-image. The 3D images and movies of phage penetration were reconstructed from the Z-stack images via a Python library Mayavi.

To test curli fiber production by the biofilm, *E. coli* strain WR3110 was grown on TSY agar plate supplemented with an amyloid dye thioflavin S[38] (40gml^{-1}) for 72 hours at 28°C. After incubation, mature biofilms were imaged using Zeiss LSM 880 confocal microscope and z-stack images (3 μm slices) of the *E. coli* biofilm were obtained. The maximum intensity 3D images were reconstructed from the Z-stack images using Zeiss Zen Black software to visualize the distribution of curli fiber within the biofilm.

Fluorescence *in situ* hybridization. To understand the mechanism behind biofilm penetration by phages in the presence of *C. gingivalis*, the curli fiber producing *E. coli* strain WR3110 with plasmid pBT1 mCherry was grown on TSY agar pad for 48 hours at 28°C. 50 μL of *C. gingivalis* suspension was spotted around the circumference of an *E. coli* biofilm and incubated at 37° C in a humid AnaeroPack System box for 24 hours. After incubation, the top layer of the agar was sliced using a scalpel. The biofilm was gently extracted from agar plates such that we remove as much agar as possible without disturbing the biofilm, and it was placed on a silane-coated microscope slides (Electron Microscopy Sciences, Hartford, PA, catalog # 63411-01).

Biofilms were fixed in 250 μL 4% paraformaldehyde in PBS (pH 7.1) using GeneFrame chambers (Thermo Scientific, Pittsburgh, PA, catalog # AB0577), and placed in a in a closed glass Tupperware box containing a beaker with 25 mL water for 2 hours at 4°C. After incubation, the biofilms were gently washed with 250 μL PBS. Subsequently, 250 μL of 1 mg/mL lysozyme in 20 mM Tris-HCl (pH 7.5) was added to the GeneFrame chamber and incubated at 37°C for 30 min in a closed glass

Tupperware box containing a beaker with 25 mL water. The lysozyme solution was replaced with a 250 μL hybridization buffer which contains 20 mM Tris-HCl [pH 7.5], 0.9 M NaCl, 20% formamide, 0.01% SDS, and 250 nM of a probe fluorescently labeled with tetrachlorofluorescein (TET). The probe targets the 16S rRNA of *Capnocytophaga* spp. (5' – TCA GTC TTC CGA CCA TTG – 3')[40,62] and was manufactured by Biosearch Technologies, Petaluma, CA.

Biofilms were incubated at 46°C for 4 hours in a closed glass Tupperware box containing 25 mL of 20% formamide. The hybridization solution was removed and biofilms were washed in 250 μL wash buffer (20 mM Tris-HCl [pH 7.5], 215 mM NaCl, 5 mM EDTA) for 15 min at 48°C. The wash solution was removed and biofilms were mounted in VectaShield vibrance antifade mounting solution (Fisher Scientific, Pittsburgh, PA, catalog # H-1700-10) for a minimum of 1 hour at 4°C prior to imaging. z-stack images (3 μm slices) were acquired using a Zeiss LSM 880 confocal microscope. Z-stack images were analyzed using ImageJ and custom Python scripts that use Scikit-image. The 3D images and movies of phage penetration were reconstructed from the Z-stack images via a Python library Mayavi.

Acknowledgements. We thank Lanying Zeng and Knut Drescher for providing strains. This research is supported by NIH R00 grant DE026826.

Author Contributions. AS and NKR conceptualized the experiments and wrote the paper. NKR performed majority of experiments and data analysis. AS performed the initial experiment for phage transportation. CAC performed the simulations. AMZ performed the FISH experiment.

Data Availability. Example datasets and custom data analysis scripts are freely available on GitHub. All additional data is available upon request.

Figure legends.

Figure 1. A swarm of *Capnocytophaga gingivalis* can actively transport phages. **(a)** trajectories from one movie show 45 phages being propelled by a *C. gingivalis* swarm. **(b)** Time-lapse images of a fluorescent lambda phage (green) being actively transported by a swarm of C. gingivalis (grey). Position of phage is shown in green, and the trajectory is shown in cyan. Scale bar = 5μm. **(c)** A frequency distribution of speed at which the phage travel is represented as both histogram and a rug plot. Inset shows the cumulative density function (CDF) of phage speed. **(d)** Mean squared displacement of the 45 phages plotted as a function of time on a log scale. The phages were tracked for ~6 minutes. The slope (α) of power law fit shows that the phages are in super diffusive state (α=1.22) where they are actively propelled by *C. gingivalis* swarms.

Figure 2. Phage delivery increases biomass clearance of the prey. (a) Mean squared displacement of the phages plotted as a function of time on a log scale. The data phages diffusing on a thin layer of liquid on a wet agar surface are shown in blue Phages diffusing in the extracellular fluid secreted by a *C. gingivalis* that is no longer motile is shown in red. **(b)** A simulation of phage particles diffusing in liquids of differing viscosity. Blue represents the viscosity of the control shown in fig. 2d and 2e. Dotted green, red, and magenta depict swarm fluid, lesquerella oil, and canola oil, respectively. **(c)** Simulations of advective diffusion of phages with different advective

velocity. Predicted transport with the calculated 1D advective velocity of a *C. gingivalis* swarm is shown in green. **(d)** Cartoons showing that in the control, phages (green) diffuse into a colony of labeled *E. coli* (red). Whereas, in the experiment they are delivered by a swarm of *C. gingivalis* (orange). **(e)** Images of the *E. coli* colony shown at two time points for the experiment and the control. This image accompanies Movies 4-8 and fig. S3 - S6 **(f)** Change in the area of the *E. coli* biomass depicted as a function of time.

Figure 3. Transport by *C. gingivalis* increases three-dimensional phage delivery within in a mature *E. coli* biofilm. A cartoon **(a)** showing a curli fiber containing a 72 h old *E. coli* biofilm (red) with phages (green). Top view **(b)** and bottom view **(c)** of the control shown. Phages are in green and blue depicts rest of the biofilm. A cartoon **(d)** of a curli fiber containing 72 h old *E. coli* biofilm (red) with phages (green) being delivered by *C. gingivalis* (yellow). Top view **(e)** and bottom view **(f)** of the biofilm with phages shown in green and blue depicts rest of the biofilm. A slice of the biofilm along with sections of the top and bottom layer are shown for the control **(g)** and after active phage delivery **(h).** Change in the area of phages along z-axis **(i)** show that after delivery by *C. gingivalis*, the maximum number of phages are found at a depth of ~60μm. in the control, greatest density of phages are found in the top layer (z = 0 μm)

Figure 4. *C. gingivalis* drills tunnels in a mature *E. coli* biofilm. (a) A 3-dimensional view of the invasion of a mature *E. coli* biofilm by *C. gingivalis. E. coli* is shown as red and *C. gingivalis* is shown in green. (**b**) An unmixed view of an image in panel a, showing only *C. gingivalis*. A zoomed in view of a small section from the image in panel b depicts finger like projections formed by the *C. gingivalis* swarm within a

mature *E. coli* biofilm. (**c**) A cartoon of the control where due to curli fiber (white), phages (green) fail to penetrate the *E. coli* biofilm (red). (**d**) A cartoon depicting that *C. gingivalis* (yellow) and phages (green) are able to penetrate the biofilm through tunnels formed by the *C. gingivalis* swarm.

Figure 1.

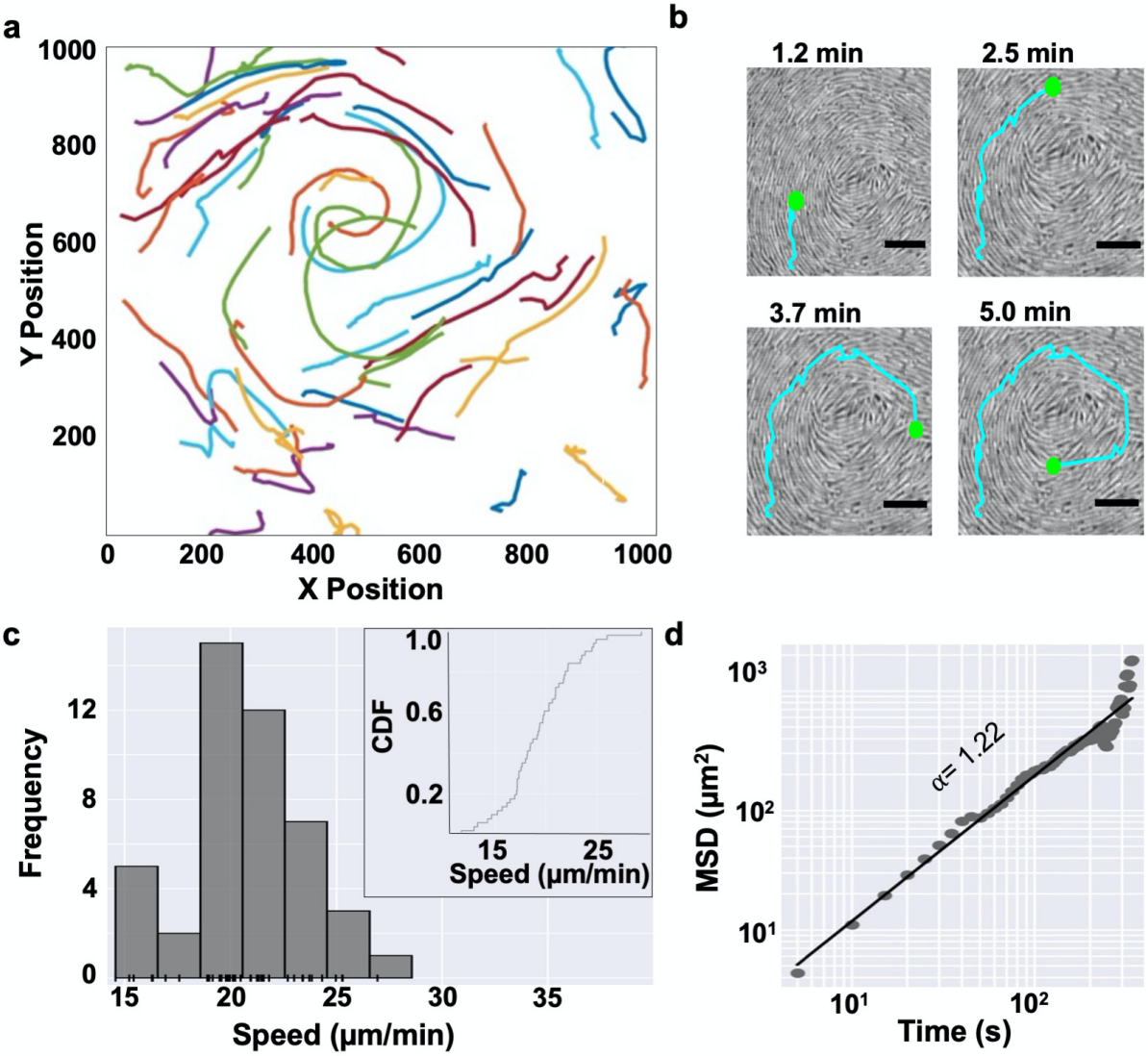

Figure 2.

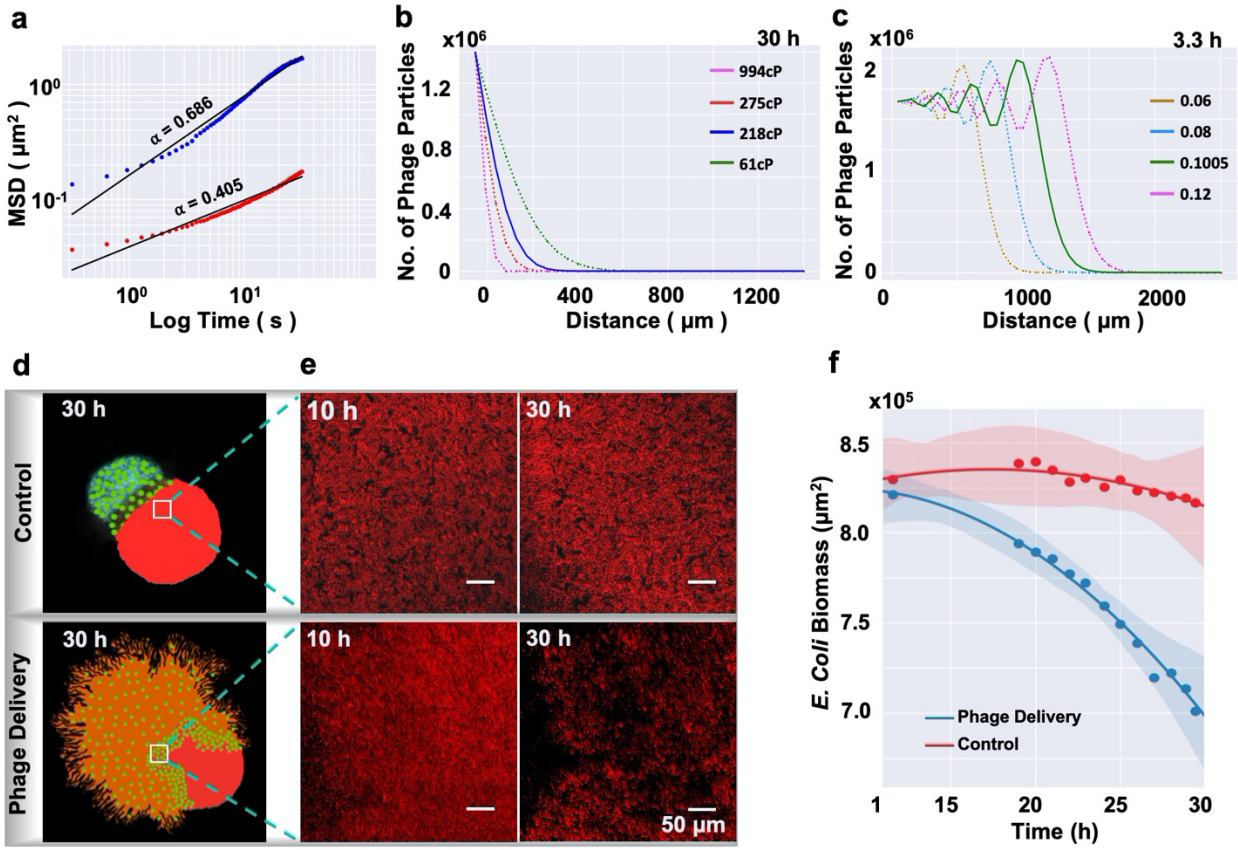
a
MSD (μm²)
α = 0.686
α = 0.405
Log Time (s)
b
30 h
No. of Phage Particles
994cP
275cP
218cP
61cP
Distance (μm)
c
3.3 h
No. of Phage Particles
0.06
0.08
0.1005
0.12
Distance (μm)
d
Control
Phage Delivery
30 h
e
10 h
30 h
50 μm
f
E. Coli Biomass (μm²)
Phage Delivery
Control
Time (h)

Figure 3.

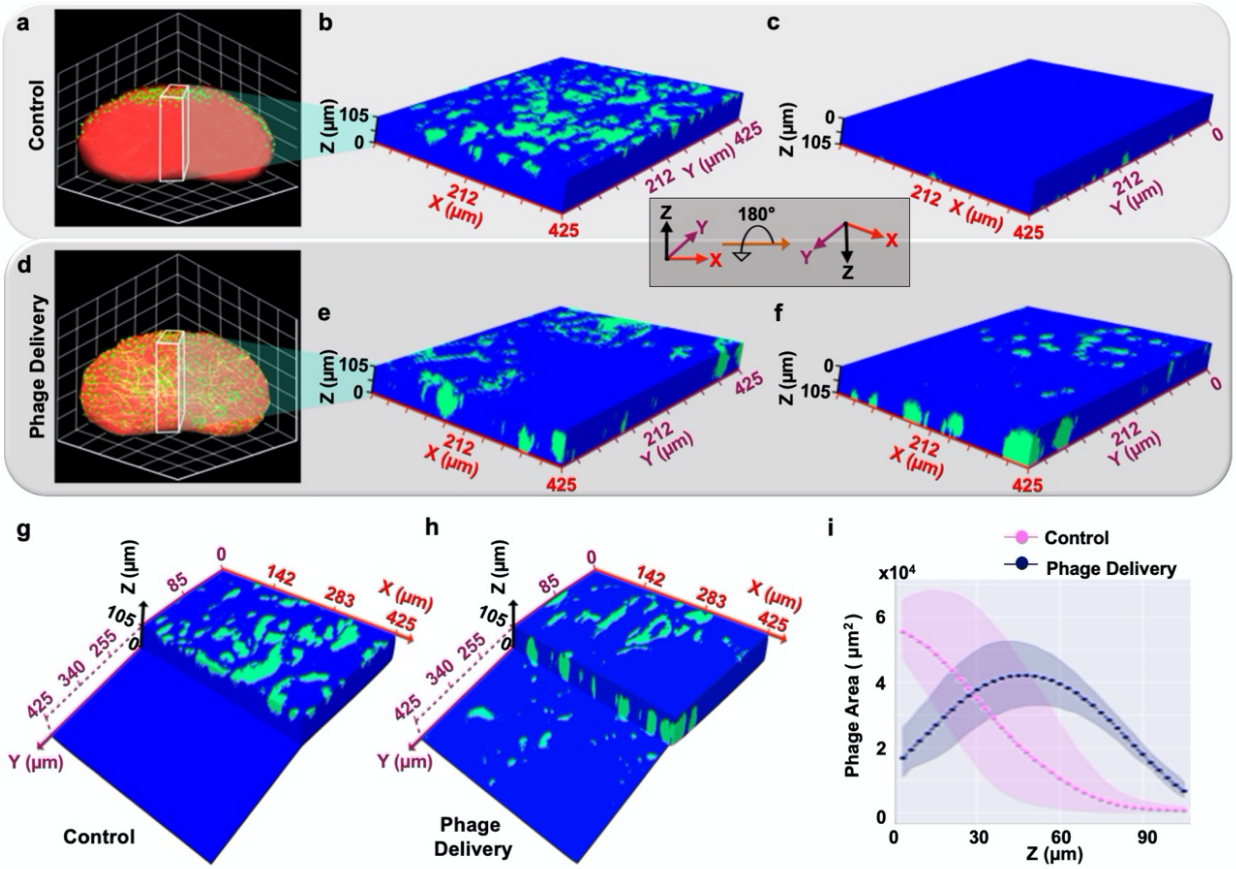

a
Control
b
c
d
Phage Delivery
e
f
Z (µm)
X (µm)
Y (µm)
180°
g
h
i
Control
Phage Delivery
Phage Area (µm²)
x10⁴
Z (µm)

Figure 4.

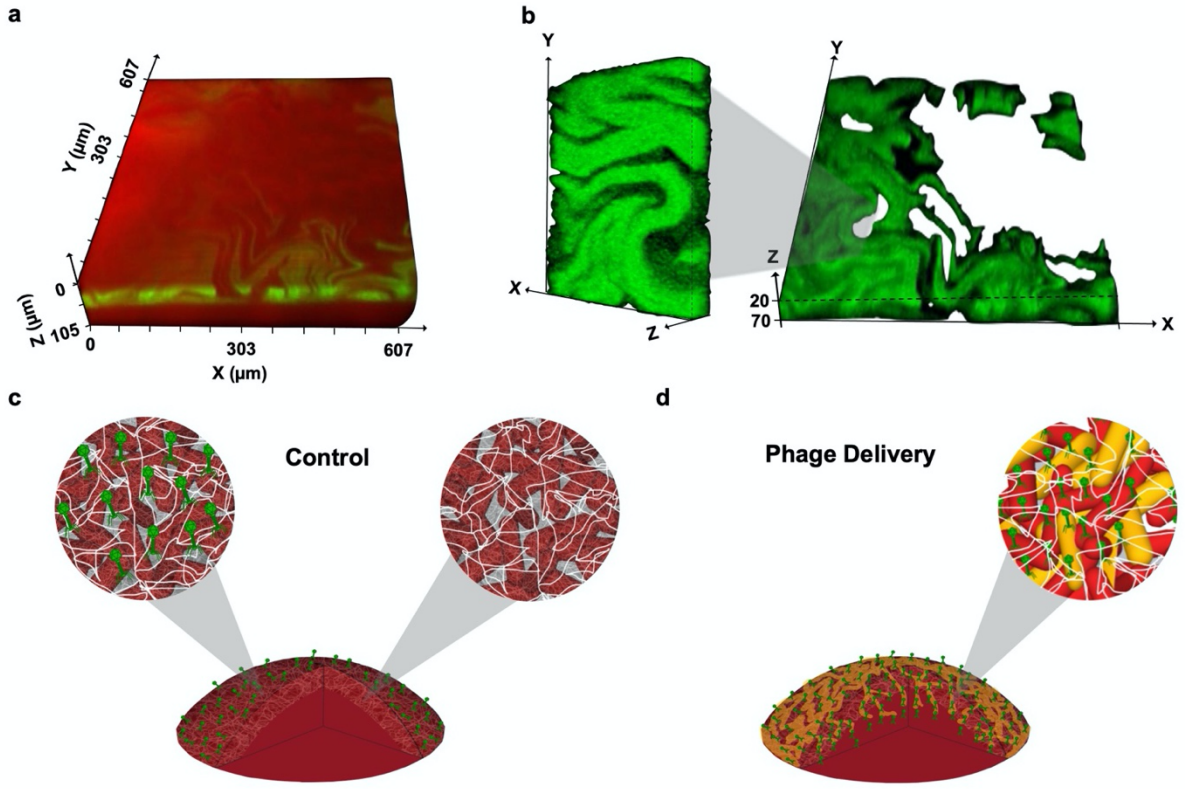
a
607
Y (µm)
303
0
Z (µm)
105
0
303
607
X (µm)
b
Y
X
Z
Y
Z
20
70
X
c
Control
d
Phage Delivery

Supplementary Information.

Supplementary movies.

Movie S1. Fluorescent lambda phage (green) being actively transported by a swarm of *C. gingivalis* (gray).

Movie S2. An example where lambda phage (green) does not adhere to a motile *C. gingivalis* cell.

Movie S3. An example where a lambda phage (green) transiently attaches to *C. gingivalis* cell and is transported as cargo.

Movie S4. Fluorescent lambda phage (green) diffusing in the thin layer of liquid on the surface of wet agar incubated with 100% relative humidity.

Movie S5. Fluorescent lambda phage (green) in the swarm fluid of a *C. gingivalis* swarm that has stopped swarming.

Movie S6. Time-lapse images of a fluorescent *E. coli* colony (red) in the diffusion control where phages are in a thin layer on a wet agar surface.

Movie S7. Time-lapse image of a fluorescent E. *coli* colony (red) in the experiment where phages are delivered by C. *gingivalis* swarms.

Movie S8. Time-lapse image of a fluorescent *E. coli* colony (red) in the control that only has *C. gingivalis*.

Movie S9. A 3-dimensional view of phage (green) penetration in a 425 μm X 425 μm X 105 μm cross section of the biofilm. Phages were diffusing in a curli fiber producing *E. coli* biofilm.

Movie 10. A 3-dimensional view of phage (green) penetration in a 425μm X 425μm X 105μm cross section of the biofilm. Phages were actively delivered to a curli fiber producing *E. coli* biofilm by a swarm of *C. gingivalis.*

Movie 11. A 3-dimensional view of a curli fiber containing *E. coli* biofilm being penetrated by a *C. gingivalis* swarm (green).

Movie 12. A 3-dimensional view of finger like projections of the tunnels formed in an *E. coli* biofilm by *C. gingivalis*.

Supplementary figure legends.

Figure S1. A swarm of *Capnocytophaga gingivalis* can actively transport phages. (a) Trajectories from all data collected show 201 phages being propelled by a *C. gingivalis* swarm. **(b)** A frequency distribution of the speed at which the 201 phages travel is represented as both histogram and a rug plot.

Figure S2. A time-lapse image of a phage particle being transiently propelled along the surface of a *C. gingivalis* cell is shown. The yellow arrow indicates the direction of motion of phage and the red arrow indicates the direction of motion of a *C. gingivalis* cell.

Figure S3. Images of the *E. coli* colony shown at different time points. Here, phages were spotted 1500 μm away from the imaged spot and were diffusing on the thin liquid layer on a wet agar surface.

Figure S4. Images of the *E. coli* colony shown at different time points. Here, phage-CG mix was spotted 1500 μm away from the imaged spot and phages are being actively delivered by a swarm of C. *gingivalis.*

Figure S5. Images of the *E. coli* colony shown at different time points. Here, only *C. gingivalis* was spotted 1500 μm away from the imaged spot. No phages were present.

Figure S6. Change in the area of the *E. coli* biomass depicted as a function of time when only *C. gingivalis* invades an *E. coli* colony. This control shows that there is no change in *E.coli* biomass due to the presence of only *C. gingivalis*.

Figure S7. A colony image taken at 30 hours after inoculation showing the interaction between *C. gingivalis* (rough) and *E. coli* (smooth

Figure S8: A maximum intensity projection (cyan) of stained curli fiber from z-stack images of an *E. coli* biofilm.

Figure S9: (a) A plaque assay shows that lambda phage does not infect *C. gingivalis*. **(b)** As a control, a plaque assay shows infection of *E. coli* by lambda phage.

Figure S1.

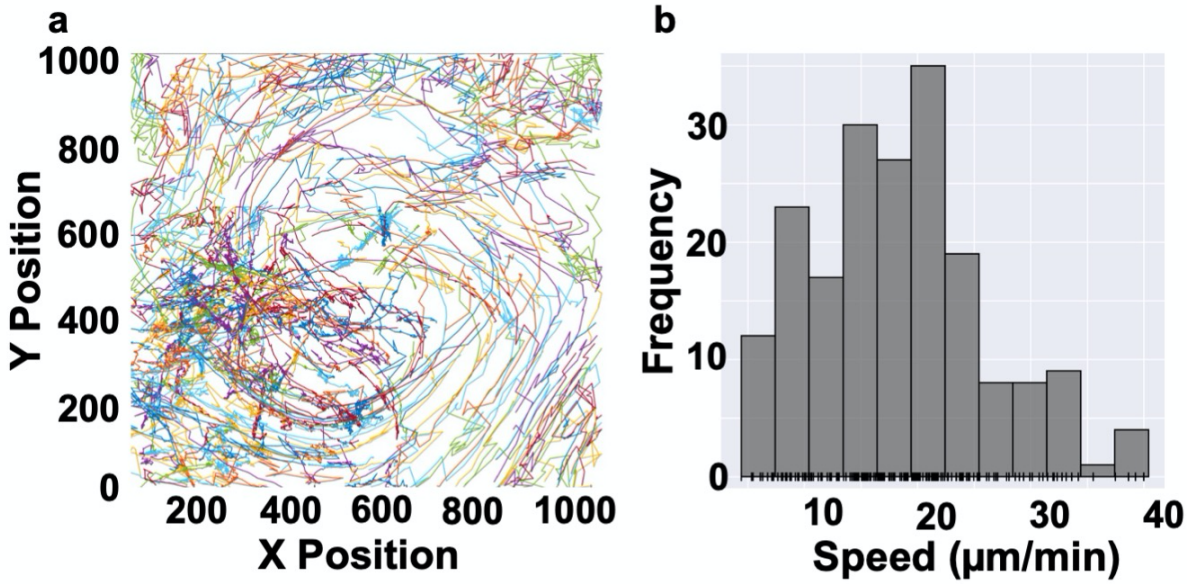

Figure S2.

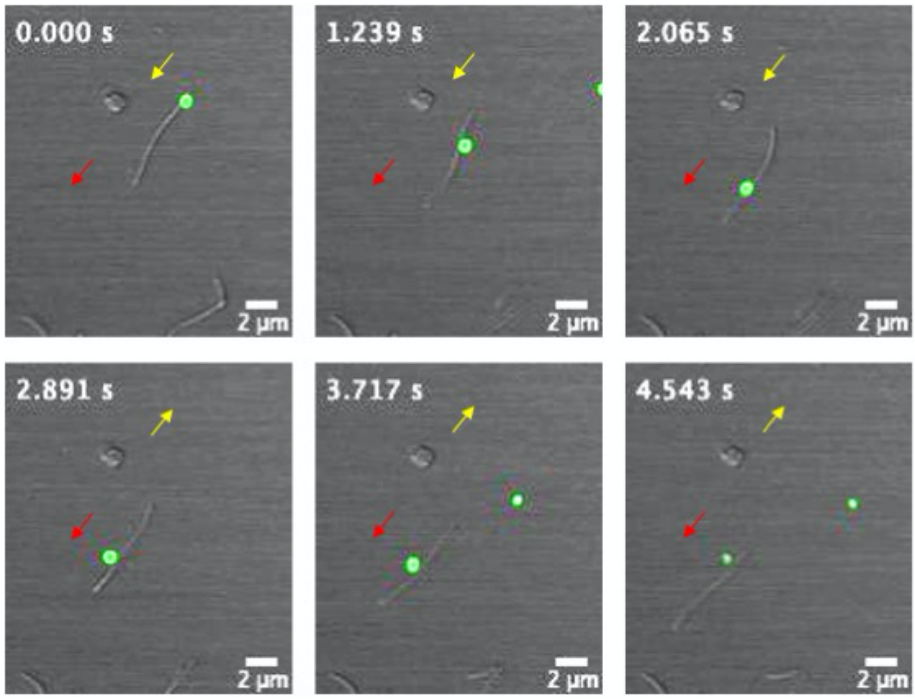

Figure S3.

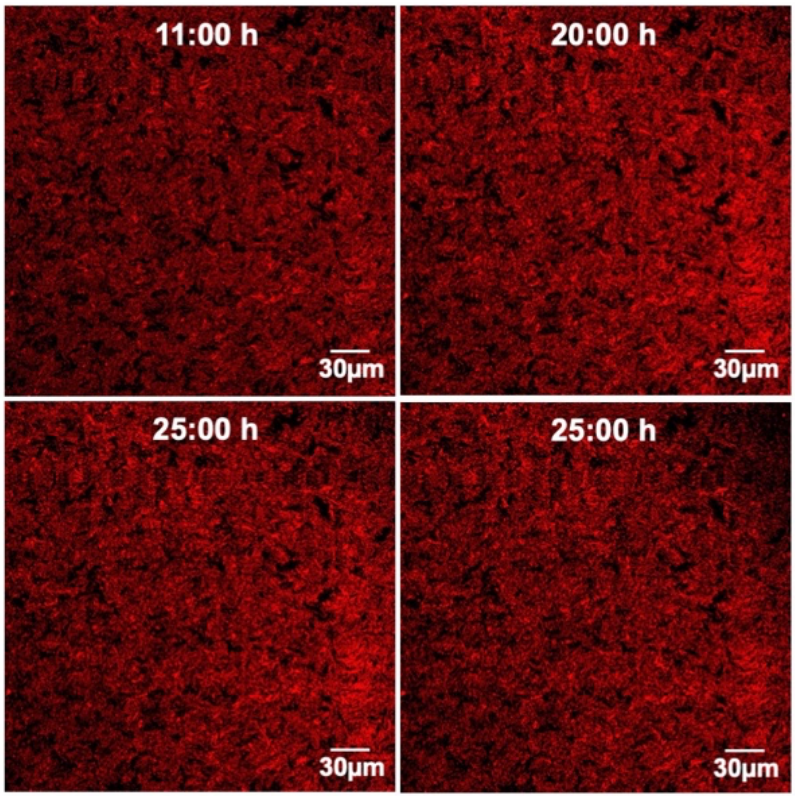

Figure S4.

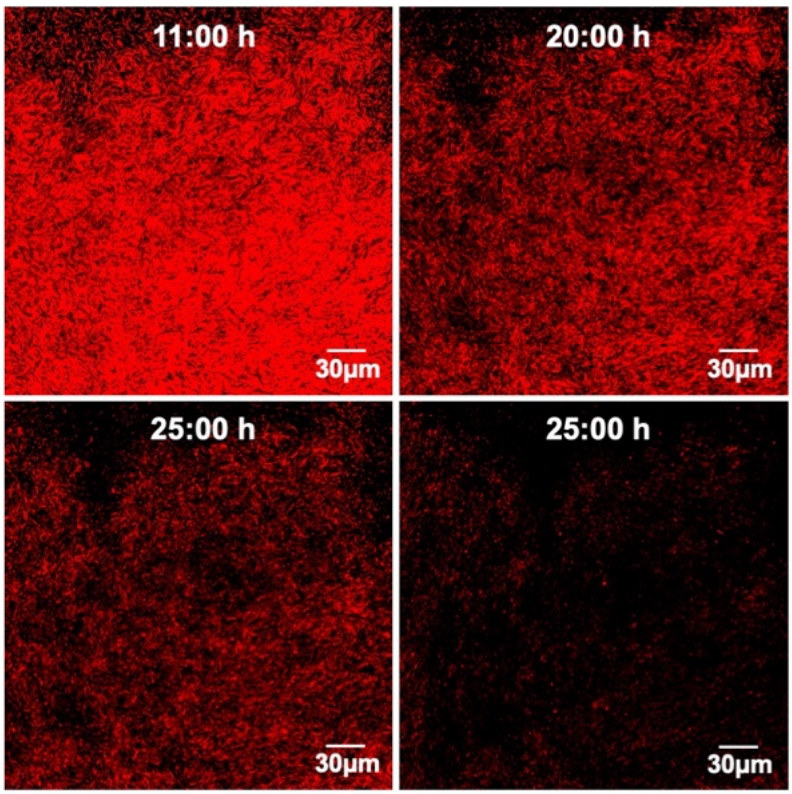

Figure S5.

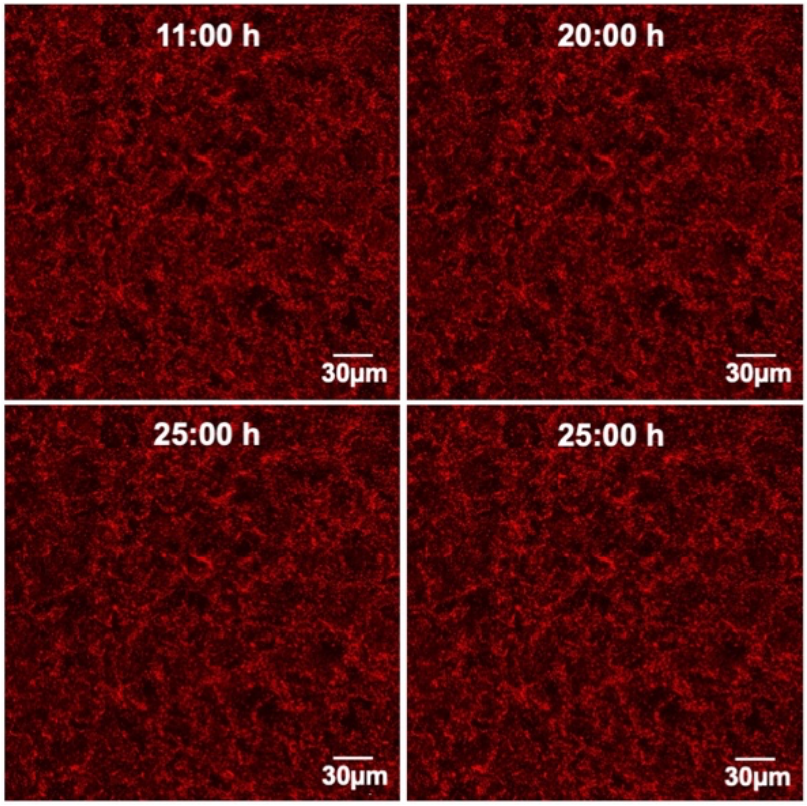

Figure S6.

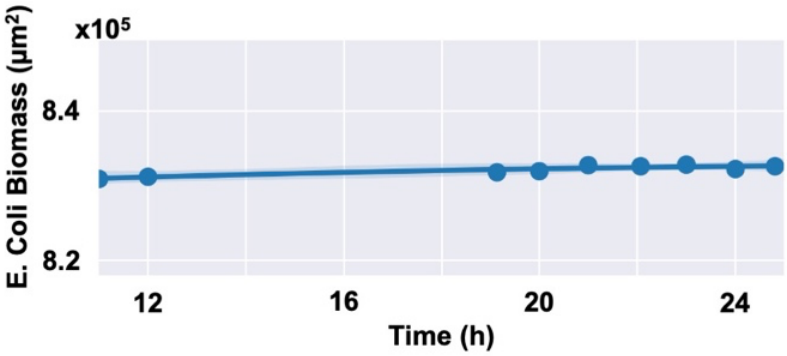

Figure S7.

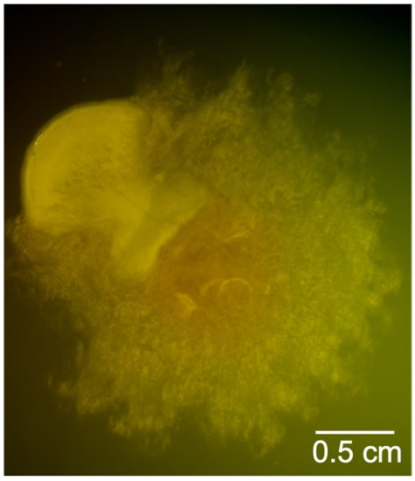

Figure S8.

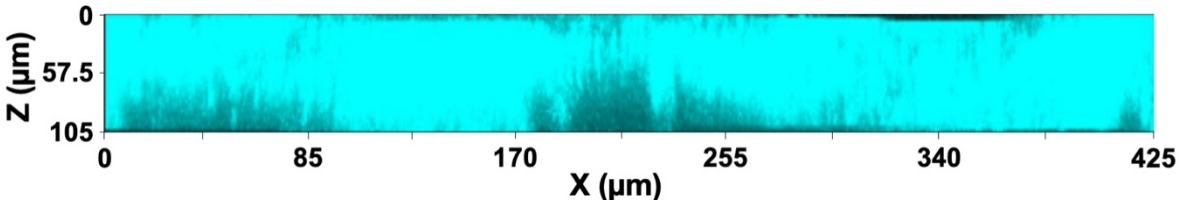

Figure S9.

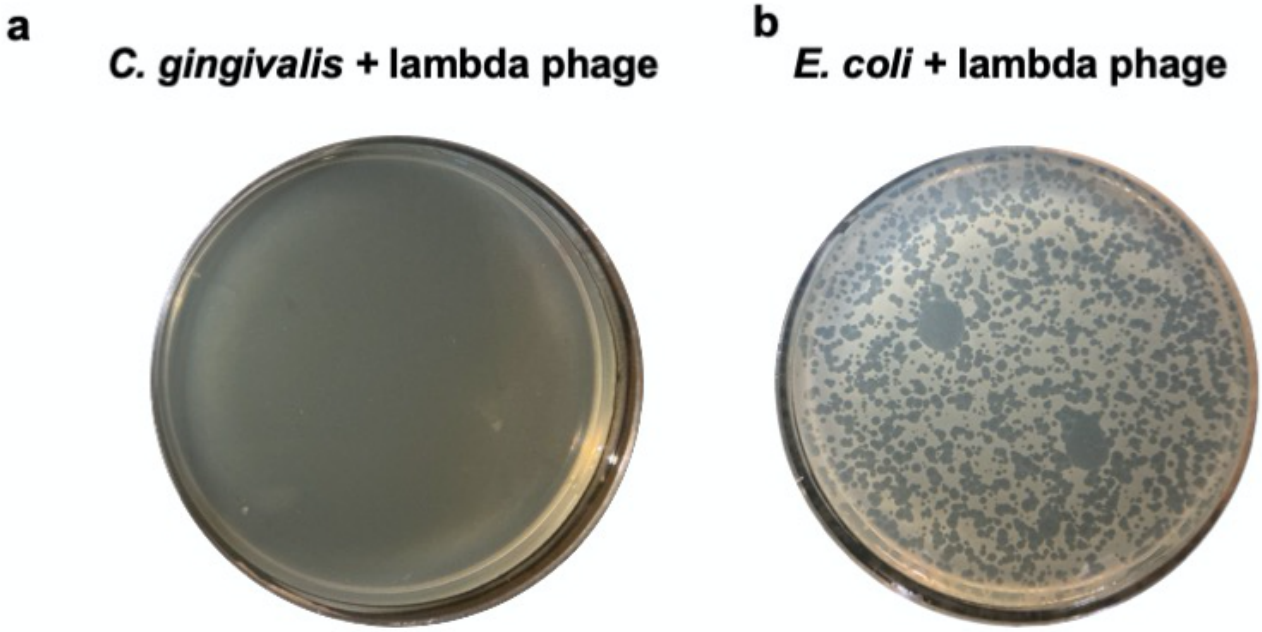

References.

1. CDC. Antibiotic Resistance Threatens Everyone. *Centers for Disease Control and Prevention* https://www.cdc.gov/drugresistance/index.html (2020).
2. Mah, T.-F. C. & O'Toole, G. A. Mechanisms of biofilm resistance to antimicrobial agents. *Trends in Microbiology* **9**, 34–39 (2001).
3. Salmond, G. P. C. & Fineran, P. C. A century of the phage: past, present and future. *Nat Rev Microbiol* **13**, 777–786 (2015).
4. Brives, C. & Pourraz, J. Phage therapy as a potential solution in the fight against AMR: obstacles and possible futures. *Palgrave Commun* **6**, 1–11 (2020).
5. Luong, T., Salabarria, A.-C., Edwards, R. A. & Roach, D. R. Standardized bacteriophage purification for personalized phage therapy. *Nat Protoc* **15**, 2867–2890 (2020).
6. Gutiérrez, D., Rodríguez-Rubio, L., Martínez, B., Rodríguez, A. & García, P. Bacteriophages as Weapons Against Bacterial Biofilms in the Food Industry. *Front. Microbiol.* **7**, (2016).
7. Dedrick, R. M. *et al.* Engineered bacteriophages for treatment of a patient with a disseminated drug-resistant Mycobacterium abscessus. *Nat Med* **25**, 730–733 (2019).
8. Wright, A., Hawkins, C. H., Änggård, E. E. & Harper, D. R. A controlled clinical trial of a therapeutic bacteriophage preparation in chronic otitis due to antibiotic-resistant *Pseudomonas aeruginosa* ; a preliminary report of efficacy. *Clinical Otolaryngology* **34**, 349–357 (2009).
9. Ujmajuridze, A. *et al.* Adapted Bacteriophages for Treating Urinary Tract Infections. *Front Microbiol* **9**, 1832 (2018).

10. McVay, C. S., Velásquez, M. & Fralick, J. A. Phage Therapy of *Pseudomonas aeruginosa* Infection in a Mouse Burn Wound Model. *Antimicrob Agents Chemother* **51**, 1934–1938 (2007).
11. Pires, D. P., Vilas Boas, D., Sillankorva, S. & Azeredo, J. Phage Therapy: a Step Forward in the Treatment of Pseudomonas aeruginosa Infections. *J Virol* **89**, 7449–7456 (2015).
12. Jault, P. *et al.* Efficacy and tolerability of a cocktail of bacteriophages to treat burn wounds infected by Pseudomonas aeruginosa (PhagoBurn): a randomised, controlled, double-blind phase 1/2 trial. *Lancet Infect Dis* **19**, 35–45 (2019).
13. Hu, J., Miyanaga, K. & Tanji, Y. Diffusion properties of bacteriophages through agarose gel membrane. *Biotechnology Progress* **26**, 1213–1221 (2010).
14. Cauda, V., Onida, B., Platschek, B., Mühlstein, L. & Bein, T. Large antibiotic molecule diffusion in confined mesoporous silica with controlled morphology. *J. Mater. Chem.* **18**, 5888–5899 (2008).
15. Roets, E. *et al.* Isolation and structure elucidation of ampicillin and amoxicillin oligomers. *Journal of Chromatography A* **303**, 117–129 (1984).
16. Anacona, J. R. & Rodriguez, I. Synthesis and antibacterial activity of cephalexin metal complexes. *Journal of Coordination Chemistry* **57**, 1263–1269 (2004).
17. Turel, I., Bukovec, P. & Quirós, M. Crystal structure of ciprofloxacin hexahydrate and its characterization. *International Journal of Pharmaceutics* **152**, 59–65 (1997).
18. Vardanyan, R. S. & Hruby, V. J. 32 - Antibiotics. in *Synthesis of Essential Drugs* (eds. Vardanyan, R. S. & Hruby, V. J.) 425–498 (Elsevier, 2006). doi:10.1016/B978-044452166-8/50032-7.
19. Earnshaw, W. C. & Harrison, S. C. DNA arrangement in isometric phage heads. *Nature* **268**, 598–602 (1977).

20. Mertens, P. The dsRNA viruses. *Virus Research* **101**, 3–13 (2004).

21. Finkelshtein, A., Roth, D., Ben Jacob, E. & Ingham, C. J. Bacterial Swarms Recruit Cargo Bacteria To Pave the Way in Toxic Environments. *mBio* **6**, e00074-15 (2015).

22. Samad, T. *et al.* Swimming bacteria promote dispersal of non-motile staphylococcal species. *ISME J* **11**, 1933–1937 (2017).

23. Muok, A. R., Claessen, D. & Briegel, A. Microbial hitchhiking: how Streptomyces spores are transported by motile soil bacteria. *The ISME Journal* 1–10 (2021) doi:10.1038/s41396-021-00952-8.

24. Shrivastava, A. *et al.* Cargo transport shapes the spatial organization of a microbial community. *Proc Natl Acad Sci USA* **115**, 8633–8638 (2018).

25. Grossart, H.-P., Dziallas, C., Leunert, F. & Tang, K. W. Bacteria dispersal by hitchhiking on zooplankton. *Proceedings of the National Academy of Sciences* **107**, 11959–11964 (2010).

26. Yu, Z. *et al.* Hitchhiking Behavior in Bacteriophages Facilitates Phage Infection and Enhances Carrier Bacteria Colonization. *Environ Sci Technol* **55**, 2462–2472 (2021).

27. Ping, D. *et al.* Hitchhiking, collapse, and contingency in phage infections of migrating bacterial populations. *ISME J* **14**, 2007–2018 (2020).

28. Jarrell, K. F. & McBride, M. J. The surprisingly diverse ways that prokaryotes move. *Nat Rev Microbiol* **6**, 466–476 (2008).

29. Harshey, R. M. Bacterial motility on a surface: many ways to a common goal. *Annu Rev Microbiol* **57**, 249–273 (2003).

30. Shrivastava, A., Roland, T. & Berg, H. C. The Screw-Like Movement of a Gliding Bacterium Is Powered by Spiral Motion of Cell-Surface Adhesins. *Biophys J* **111**, 1008–1013 (2016).
31. Faure, L. M. *et al.* The mechanism of force transmission at bacterial focal adhesion complexes. *Nature* **539**, 530–535 (2016).
32. Flavobacterium johnsoniae PorV Is Required for Secretion of a Subset of Proteins Targeted to the Type IX Secretion System. *Journal of Bacteriology* https://journals.asm.org/doi/abs/10.1128/JB.02085-14.
33. Flavobacterium johnsoniae RemA Is a Mobile Cell Surface Lectin Involved in Gliding. *Journal of Bacteriology* https://journals.asm.org/doi/abs/10.1128/JB.00588-12.
34. Berg, H. C. The Rotary Motor of Bacterial Flagella. *Annual Review of Biochemistry* **72**, 19–54 (2003).
35. Shrivastava, A. & Berg, H. C. A molecular rack and pinion actuates a cell-surface adhesin and enables bacterial gliding motility. *Sci Adv* **6**, eaay6616 (2020).
36. Nakane, D., Odaka, S., Suzuki, K. & Nishizaka, T. Large-Scale Vortices with Dynamic Rotation Emerged from Monolayer Collective Motion of Gliding *Flavobacteria*. *J Bacteriol* **203**, (2021).
37. Vidakovic, L., Singh, P. K., Hartmann, R., Nadell, C. D. & Drescher, K. Dynamic biofilm architecture confers individual and collective mechanisms of viral protection. *Nat Microbiol* **3**, 26–31 (2018).
38. Serra, D. O., Richter, A. M., Klauck, G., Mika, F. & Hengge, R. Microanatomy at cellular resolution and spatial order of physiological differentiation in a bacterial biofilm. *mBio* **4**, e00103-00113 (2013).

39. Steward, G., Smith, D. & Azam, F. Abundance and production of bacteria and viruses in the Bering and Chukchi Seas. *Mar. Ecol. Prog. Ser.* **131**, 287–300 (1996).

40. Welch, J. L. M., Rossetti, B. J., Rieken, C. W., Dewhirst, F. E. & Borisy, G. G. Biogeography of a human oral microbiome at the micron scale. *PNAS* **113**, E791–E800 (2016).

41. Zeng, L. *et al.* Decision making at a subcellular level determines the outcome of bacteriophage infection. *Cell* **141**, 682–691 (2010).

42. Hennell James, R. *et al.* Structure and mechanism of the proton-driven motor that powers type 9 secretion and gliding motility. *Nat Microbiol* **6**, 221–233 (2021).

43. Lauber, F., Deme, J. C., Lea, S. M. & Berks, B. C. Type 9 secretion system structures reveal a new protein transport mechanism. *Nature* **564**, 77–82 (2018).

44. Wu, Y., Hosu, B. G. & Berg, H. C. Microbubbles reveal chiral fluid flows in bacterial swarms. *Proc Natl Acad Sci U S A* **108**, 4147–4151 (2011).

45. Zhang, R., Turner, L. & Berg, H. C. The upper surface of an Escherichia coli swarm is stationary. *Proc Natl Acad Sci U S A* **107**, 288–290 (2010).

46. Shkoporov, A. N. & Hill, C. Bacteriophages of the Human Gut: The 'Known Unknown' of the Microbiome. *Cell Host Microbe* **25**, 195–209 (2019).

47. Szafrański, S. P., Slots, J. & Stiesch, M. The human oral phageome. *Periodontol 2000* **86**, 79–96 (2021).

48. Leadbetter, E. R., Holt, S. C. & Socransky, S. S. Capnocytophaga: New genus of gram-negative gliding bacteria I. General characteristics, taxonomic considerations and significance. *Arch. Microbiol.* **122**, 9–16 (1979).

49. *Random Walks in Biology*. (1993).

50. Noureddini, H., Teoh, B. C. & Davis Clements, L. Densities of vegetable oils and fatty acids. *J Am Oil Chem Soc* **69**, 1184–1188 (1992).
51. Rojas, E. E. G., Coimbra, J. S. R. & Telis-Romero, J. Thermophysical Properties of Cotton, Canola, Sunflower and Soybean Oils as a Function of Temperature. *International Journal of Food Properties* **16**, 1620–1629 (2013).
52. Rebbapragada, A. *et al.* The Aer protein and the serine chemoreceptor Tsr independently sense intracellular energy levels and transduce oxygen, redox, and energy signals for Escherichia coli behavior. *Proc Natl Acad Sci U S A* **94**, 10541–10546 (1997).
53. Laganenka, L., Colin, R. & Sourjik, V. Chemotaxis towards autoinducer 2 mediates autoaggregation in Escherichia coli. *Nat Commun* **7**, 12984 (2016).
54. Jani, S., Seely, A. L., Peabody V, G. L., Jayaraman, A. & Manson, M. D. Chemotaxis to self-generated AI-2 promotes biofilm formation in Escherichia coli. *Microbiology* **163**, 1778–1790 (2017).
55. Park, S. *et al.* Influence of topology on bacterial social interaction. *Proc Natl Acad Sci U S A* **100**, 13910–13915 (2003).
56. Saragosti, J. *et al.* Directional persistence of chemotactic bacteria in a traveling concentration wave. *Proc Natl Acad Sci U S A* **108**, 16235–16240 (2011).
57. Fu, X. *et al.* Spatial self-organization resolves conflicts between individuality and collective migration. *Nat Commun* **9**, 2177 (2018).
58. Colin, R., Drescher, K. & Sourjik, V. Chemotactic behaviour of Escherichia coli at high cell density. *Nat Commun* **10**, 5329 (2019).
59. Partridge, J. D., Nhu, N. T. Q., Dufour, Y. S. & Harshey, R. M. Escherichia coli Remodels the Chemotaxis Pathway for Swarming. *mBio* **10**, (2019).

60. Matinkhoo, S., Lynch, K. H., Dennis, J. J., Finlay, W. H. & Vehring, R. Spray-dried Respirable Powders Containing Bacteriophages for the Treatment of Pulmonary Infections. *Journal of Pharmaceutical Sciences* **100**, 5197–5205 (2011).
61. Shao, Q. *et al.* Coupling of DNA Replication and Negative Feedback Controls Gene Expression for Cell-Fate Decisions. *iScience* **6**, 1–12 (2018).
62. Zijnge, V. *et al.* Oral Biofilm Architecture on Natural Teeth. *PLoS ONE* **5**, e9321 (2010).